2012 IEEE 4th International Symposium on Plant Growth Modeling, Simulation, Visualization and Applications

Simulating Plant Plasticity under Light Environment: A Source-Sink Approach

Haoyu Wang†, Mengzhen Kang** and Jing Hua*
*State Key Laboratory of Management and Control for Complex Systems,
Institute of Automation, Chinese Academy of Sciences
Email: mengzhen.kang@ia.ac.cn
†LIAMA, Institute of Automation, Chinese Academy of Sciences

***Abstract*—Simulation of plant structure competing for light source has mostly been done by directly modifying plant structure according to light interception. Functional-structural plant models, however, emphasize the influence of light interception on biomass production, and consequently plant structure. In this paper, we integrate a light distribution model with GreenLab model, which used Beer-Law in computing biomass production. By replacing Beer-Law with a light interception model for biomass production, the combined model was able to simulate the effect of light condition on plant structure through source-sink regulation. The positive and negative sides of this approach are discussed.**

***Keywords*-Plant Growth; Light Environment; Source-Sink; Photon Mapping**

I. Introduction

Light environment plays a key role for plant growth and development. Light interception is a key topic not only in plant growth modeling [1], but also in plant visualization [2]. In plant growth modeling, light interception is computed either by an empirical Beer-Law approach using leaf area index, or by summing up the light interception from individual organs, the latter taking into account the detailed description of plant structure.

Functional-Structural Plant Models (FSPMs) [3], are originated by combining Process-Based Model with 3D simulation of plant structure. A natural application is the computation of biomass production according to the interception light by plant organs [4], which can be used for comparing different genotypes [5]. Calibration of virtual light environment, which is a tedious work, has been done on open field for maize [6], rice[7] and greenhouse environment [8]. However, light interception is generally computed based on observed plant structure, and its feedback on plant structure is rarely simulated.

On the other hand, it is well recognized that light condition influences on plant structure and function, and efforts have been made on simulating plant response to different light environment. In plant modeling, Evers et al. [9] linked the simulated red: far red ratio in light component to numbers of wheat tillers; Kahlen et al. [10] simulated the cucumber leaf direction according to the light source. In all these approaches, the light environment modifies directly the plant structure. Instead, Cournède [11] simulated plasticity of plant structures in competition to light based on source-sink regulation, but the effect of 3D plant structure and light environment can not be explicitly taken into accounted. For plant visualization, light environment is used to simulate the visual effects of plant that search the light source [12]. Hua and Kang [13] introduced bud breakout rule under light environment to simulate plant structure competing for light.

In this paper, we attempt to simulate the effect of light distribution on biomass production and consequently plant structure, through a source-sink approach. Photon mapping method [14] is selected to simulate the light environment, which is an efficient method for representing light environment in complex scene. GreenLab model is used for simulating organ production, organ growth and 3D plant structure. The implementation of system is done in Qingyuan software [15].

This paper is organized as follows: Sec. II presents the method of simulating light interception and its application in GreenLab model. Sec. III presents the simulation results. Conclusion and brief discussion are given in the last section.

II. Method

A. GreenLab Model for Trees

In this study, GreenLab model for trees [16] is used, in which the plant development is dependent on the dynamic relationship between biomass demand and supply. Biomass production Q_{B} is modeled using Beer-Law-analog equation:

$$\begin{cases} Q_{\mathrm{B}}(n) = E_{\mathrm{B}}(n)\, S_{\mathrm{p}} \left(1 - \exp\left(-k \frac{S(n)}{S_{\mathrm{p}}}\right)\right) \\ Q_{\mathrm{B}}(0) = Q_{\mathrm{seed}} \end{cases} \quad (1)$$

where $E_{\mathrm{B}}(n)$ is a variable representing the plant local environment at growth cycle n; S_{p} is the total ground projection area available of the crown for plant. k is a light extinction coefficient to quantify attenuation process of light penetrating into the canopy. $S(n)$ is the total green leaf surface area at growth cycle n. Q_{seed} is the initial biomass. The ratio of $S(n)$ to S_{p} can be considered as local leaf area index (LAI) [16] adapted to individual plants. In GreenLab, S_{p} reflect the effect of competition with neighbors and the final effect on biomass production (Eqn. 1). An alternate way is to establish link between light environment and biomass production by light distribution model. For trees or crops of low density, an allometric relationship can be found between S_p and $S(n)$ [16], as shown in Eqn. 2:

$$S_\mathrm{p} = S_{\mathrm{p}0}\left(\frac{S(n)}{S_{\mathrm{p}0}}\right)^{\sigma} \tag{2}$$

where $S_{\mathrm{p}0}$ and σ are two parameters.

At each growth cycle (GC), the amount of biomass allocated to an organ o of physiological age p at plant age n is calculated as follows:

$$q_p^o(n) = P_p^o \cdot \frac{Q_\mathrm{B}(n)}{D(n)} \tag{3}$$

where P_p^o is the sink strength of organ o of physiological age p; $D(n)$ is the plant demand at growth cycle n, which is the total sink strength of organs. At growth cycle n, the total number of new branches sprouted by metamer of physiological age p bearing buds of physiological age k, denotes $B_p^k(n)$ is given by the following Eqn. 4:

$$B_p^k(n) = \begin{cases} \left[M_p^k(n)\cdot\lambda\right] & where \;\; 0 \le \lambda < 1 \\ M_p^k(n) & where \;\; \lambda \ge 1 \end{cases} \tag{4}$$

where for a real number x, $[x]$ represents its round value. $M_p^k(n)$ denotes the number of positions in axis potentially bearing that kind of branches. λ is a positive number given by Eqn. 5:

$$\lambda = \psi \cdot \frac{Q_B(n)}{D(n)} \tag{5}$$

where ψ is a model parameter (a positive real number). It is hypothesized that this ratio of Q/D characterizes the level of trophic competition inside the plant [16]. Number of new branches have effect on plant 3D shape, and it influence on number of organs playing role of source and sink in future. With this characteristic, it is possible to simulate the feedback between local light environment and plant growth.

B. Photon Mapping

In photon mapping [14], light propagation is simulated by tracing light particles (i.e. photons) originated from light source. When a photon strikes on an organ, it can be absorbed, reflected, transmited or diffused according to the material property of the organ. To accelerate the collision detection between a photon and an organ surface, bounding volume hierarchy (BVH) method [17] is used: instead of detecting whether a photon collides with every object in the complex scene, a regular bounding volume (e.g. a cubic) of this object is used for collision detection. Each individual organ is wrapped in a bounding volume, which is leafy node in a data structure of binary tree. These nodes are then grouped as small sets and enclosed within larger bounding volumes. With such hierarchy, during collision testing, a small set does not need be examined if its parent volume does not intersect with the rays, which reduces the time complexity.

To start, photons are emitted from sky hemisphere, as shown in Fig. 1. The sky hemisphere light environment could be simulated by $N_\mathrm{A} \cdot N_\mathrm{Z} + 1$ sampling point light sources (including one peak-point of the sky hemisphere), where N_A and N_Z denote the number of sampling for altitude and azimuth angles respectively. It is supposed that each sampling point cast N_p rays into the hemisphere. At each growth cycle, there are total N_r rays projected into the scene:

$$N_\mathrm{r} = (N_\mathrm{A} \cdot N_\mathrm{Z} + 1) \cdot N_\mathrm{p} \tag{6}$$

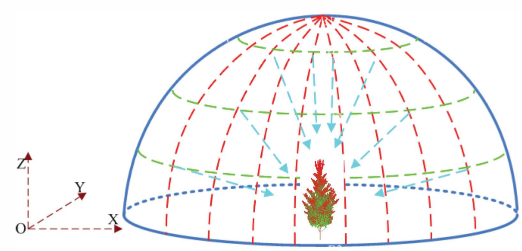

Figure 1. A sky hemisphere emitting photons to simulate isotropic light environment for plants.

To avoid emitting photons that never collide any objects, the initial directions of the outgoing photons are constrained: instead of sending out photons in random directions, they are sent in the direction of the largest BVH occupying all of the objects in the scene. The space for which the photons are emitted is bigger than the largest BVH in order to eliminate the boundary effect. When a photon strikes on the surface of an organ, a random number produced by Russian roulette method is used to determine its fate according to the probabilities of reflecting, absorbing, transmitting, or diffusing.

Photon map is a data structure containing information about all photons hits, and this information can be used to estimate efficiently the light intensity in canopy. KD-tree, which is a space-partitioning data structure for organizing points in a k-dimensional space, is used to store static photon information and to provide efficient way of locating neighboring photons[14].

To estimate the light intensity around a leaf (E_L, $\mathrm{W}\cdot\mathrm{m}^{-2}$), we search a neighborhood of radius r containing n incoming photons. E_L is calculated as in Eqn. 7

$$E_\mathrm{L} = \sum_{i=0}^{n} \frac{\Phi_i}{A}, \tag{7}$$

where Φ_i is the power of an incoming photon ($\mathrm{J}\cdot\mathrm{s}^{-1}$), A is the leaf area (m^2, $A = \pi r^2$). Given a light intensity above canopy E_C ($\mathrm{W}\cdot\mathrm{m}^{-2}$), the power of a photon is calculated

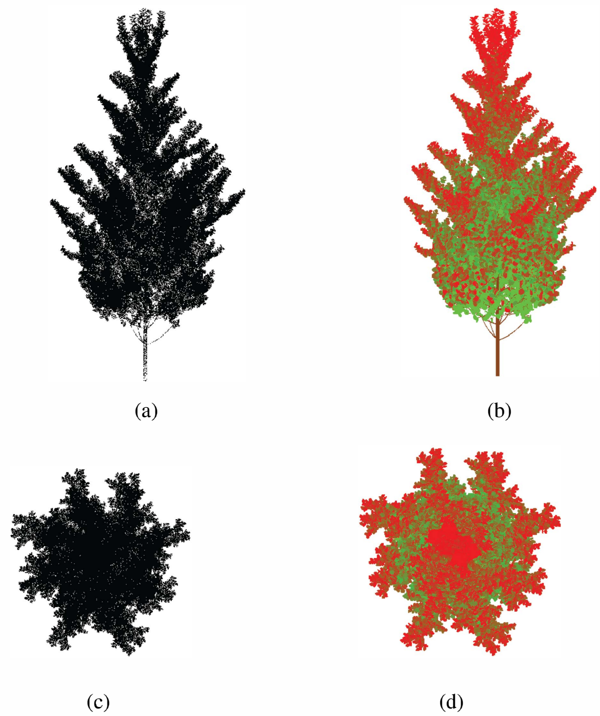

Figure 2. Photon map (a, c) obtained with scheme A-1(Table I) and light intensity E_{B} (Eqn. 8);(b,d): red color means higher light intensity.

as $\Phi_i = E_{\mathrm{C}} \cdot A_{\mathrm{C}}/T$, where A_{C} is the projecting area of the scene and T is the total number of photons.

Since Photo Mapping was originally used in rendering for computer graphics, E_{L} was used only to evaluate the relative light intensity in scene, but not the real light intensity. For photosynthesis model, absolute light intensity is necessary. The absolute light intensity E_{B} is computed from the relative light intensity (E_{L}) by assuming a maximum light intensity ($\tau_{\max}$) above canopy and a minimum light intensity ($\tau_{\min}$) inside canopy, as in Eqn. 8:

$$E_{\mathrm{B}} = (1 - \frac{E_{\mathrm{L}}}{E_{\mathrm{L}}^{\max}}) \cdot (\tau_{\max} - \tau_{\min}) + \tau_{\min} \tag{8}$$

Where $E_{\mathrm{L}}^{\max}$ is the maximal value of E_{L} of all blades. Instead of calculating the surface light intensity in computer graphics, we focus on the light intensity inside the canopy. As photons record the interception of rays by organs, for blades inside the canopy, the amount of neighboring photons denotes level of occlusion by surrounded organs. The more photons are found in the neighborhood of a leaf, the less the blade is visible from outside.

C. Photosynthesis Model

A generalized light-response curve is used to compute instantaneous assimilation rate (I, $\mu\mathrm{mol}\ \mathrm{CO_2} \cdot \mathrm{m}^{-2} \cdot \mathrm{s}^{-1}$), using a non-rectangular hyperbola [18]:

$$I = \frac{\alpha E + I_m + R_d - \sqrt{(\alpha E + I_m + R_d)^2 - 4\theta\alpha E\,(I_m + R_d)}}{2\theta} - R_d, \tag{9}$$

where E is the Photosynthesis Photon Flux Density (PPFD) of PAR ($\mu\mathrm{mol\ photons} \cdot \mathrm{m}^{-2} \cdot \mathrm{s}^{-1}$), computed by multiplying E_{B} (Eqn. 8) and the leaf efficiency for energy utilization (β, 0-1). Note the value E_{B} was converted from $\mathrm{W} \cdot \mathrm{m}^{-2}$ into $\mu\mathrm{mol\ photons} \cdot \mathrm{m}^{-2} \cdot \mathrm{s}^{-1}$ by multiplying a factors of 4.57 [19]). I_m and R_d are light saturation photosynthetic rate and leaf dark respiration rate respectively ($\mu\mathrm{mol}\ \mathrm{CO_2} \cdot \mathrm{m}^{-2} \cdot \mathrm{s}^{-1}$), α is the apparent quantum yield ($0.03 - 0.07$, $\mathrm{mol}\ \mathrm{CO_2} \cdot \mathrm{mol}^{-1}$ photons [20]), which is the ratio of the net photosynthetic rate to the number of photons. θ is the convexity of the light response curve (0-1, dimensionless). It is assumed that I_m is between 4.5 to 19.5 ($\mu\mathrm{mol}\ \mathrm{CO_2} \cdot \mathrm{m}^{-2} \cdot \mathrm{s}^{-1}$) [18]. Dark respiration rate is about 7% of peak photosynthesis [21].

Assuming that leaf is the only biomass producer at a given growth cycle, total biomass production is computed as in Eqn. 10.

$$Q_L(n) = \delta_t \gamma \sum_{i=1}^{N_B(n)} I_i(n) s_i(n), \tag{10}$$

where γ is a conversion coefficient from assimilate to dry mass, δ_t is the duration of a growth cycle (s), $N_B(n)$ denotes the total number of leaves in the plant. $I_i(n)$ and $s_i(n)$ are assimilation rate and leaf area of i^{th} individual leaf respectively.

D. Calibrating Photosynthesis Model

Eqn. 10 can be an alternate way of computing biomass production in GreenLab. In order to test whether the two approaches (Eqn. 1 and Eqn. 10) can give close results, given the same geometrical structure, parameters in Eqn. 9 (α, β, I_m, θ) and Eqn. 10 (δ_t) are estimated by fitting the output of biomass production by Eqn. 1.

Root Mean Square Error (RMSE) and Normalized Root Mean Square Error (NRMSE)[22] was computed to evaluate the fitting performance :

$$RMSE = \sqrt{\frac{\sum_{i=1}^{N}(x_L - x_B)^2}{N}} \tag{11}$$

$$NRMSE = \sqrt{\frac{\sum_{i=1}^{N}(x_L - x_B)^2}{\sum_{i=1}^{N}(x_B - \bar{x}_B)^2}} \tag{12}$$

Where x_{B} and x_{L} are biomass production obtained by Eqn. 1 and Eqn. 10 respectively. $\bar{x}_{\mathrm{B}}$ is the mean value of x_{B} $(i = 1, ..., N)$.

The RMSE was used to analyse the average difference between biomass production obtained by Eqn. 1 and Eqn. 10. If the value of the RMSE was small, then the results were close to each other. The NRMSE was used to compare the accuracy between results mentioned above which have different units and ranges. If the value of NRMSE was small, then results were closer to each other.

III. Results for Effect of light on biomass production

A. Photon Map

At each growth cycle, 10,001,000 rays are emitted to a scene containing a single tree. Photons hitting on the plant are saved in the photon map. Fig. 2(a) and Fig. 2(c) show a photon map at 25 GC, which includes 70,347 organs. Each ray bounces less than 15 times and there are total of 265,452,000 photons in the largest BVH, with 325,922 photons hitting on the plant. For this plant, collision detection of photons costs 21.1s using a Intel 4 core processor (2.13GHz).

The light intensity (E_{B}, Eqn. 8) for each leaf is shown in Fig. 2(b) and Fig. 2(d). Different colors are used to visually distinguish light intensity. Red means being lightened while green means being shaded.

In order to evaluate the algorithm, different schemes of ray emission are tested, as shown in Table I, using different number of light sources. The computational bottleneck lies in the estimation of light intensity. Fig. 3 shows the results of biomass production (Eqn. 10) are closed with different number of photons emitted, while the simulation time can be dramatically different. While bigger neighborhood size leads to more computational time, Fig. 4 shows that the search radius of neighborhood has little effect on the biomass production. However, for the plant stand, it is useful to enlarge search radius in order to consider the occlusion by surrounding trees.

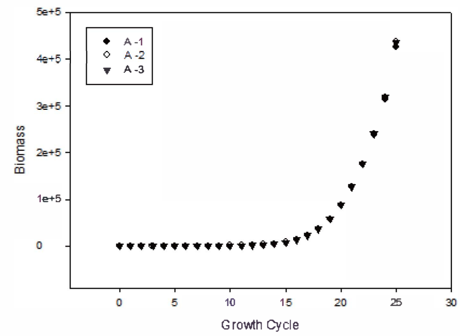

Figure 3. Biomass production obtained under different schemes on number of point light sources (Table I). Neighborhood size is $80R$, where R denotes the radius of envelop ball for a blade.

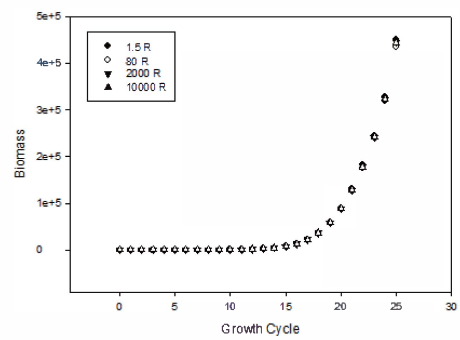

Figure 4. Biomass production obtained under different neighborhood size: 1.5 R, 80 R, 2000 R, 100000 R. R denotes the radius of envelop ball for a blade. N_{P}=10000, N_{A}=10, N_{Z}=10.

B. Fitting photosynthesis model

Using the virtual tree in Fig. 2, the parameters in Eqn. 9 and Eqn. 10 are estimated in order that the biomass production from Eqn. 1 and Eqn. 10 are similar. Fig. 5 shows such a fitting result. Remind that both results are computed from the same plant structure. It can be seen that production obtaining by summing photosynthetic production from individual leaves can be close with that from Beer-Law based approach. When the value of parameter σ is approaching 1.0, which means biomass production is proportional to leaf area, the fitting result is the best.

Table I

DIFFERENT SCHEMES OF RAY EMISSION (A-1, A-2 AND A-3). EACH POINT LIGHT SOURCE SENDING 1000 RAYS TO THE BIGGEST BVH IN THE SCENE (N_{p}=1000). PLANT AGE IS 25 CYCLES. IN SCHEME A-1,HIGHER NUMBER OF RAYS ARE EMITTED.

Scheme	A-1	A-2	A-3
Number of samples for Altitude angle (N_{A})	100	10	10
Number of samples for Azimuth angle (N_{Z})	100	100	10
Total number of rays (N_{r})	10001000	1001000	101000
Time for emitting photons (s)	21.1	1.615	0.19
Time for building KD tree (s)	0.45	0.006	0.001
Time for estimating light intensity (s)	548.661	16.086	2.24
Total number of photons	2.65E+08	2.88E+07	2.90E+06
Number of photons on plant	325922	15443	1588

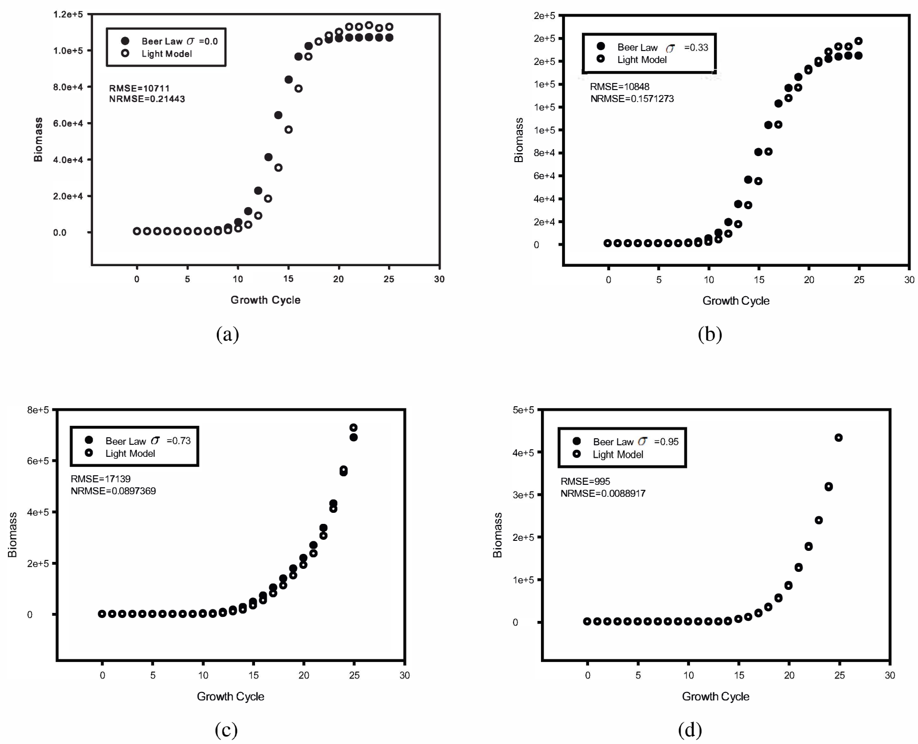

Figure 5. Fitting biomass production from light model (Eqn. 10) with Beer-Law (Eqn. 1) during plant growth: (a) σ=0.0, RMSE=10711, NRMSE=0.09405; (b) σ=0.33, RMSE=10848, NRMSE=0.06117; (c) σ=0.73, RMSE=17139, NRMSE=0.02353; (d) σ=0.95, RMSE=995, NRMSE=0.00229;

C. Simulating tree competition under Isotropic Light Condition

The morphological structure of the trees are affected by the local environment, especially neighborhood competition even under isotropic light environment. In Fig. 6, it is observed that the tree in the middle grows less and has a smaller crown than the surrounding trees as it receives less light. Planting density, which affect local light environment, plays a role on plant morphology. The greater the density, the greater effect the trees have with each other.

D. Simulating tree competition under Anisotropic Light Resource

Here we simulate the competition for light source between two neighboring trees driven by anisotropic light source, as in Fig. 7. The point light locates at the top left-hand side and the tree in the left receives more light. According to Eqn. 4, the change of the number of organs, e.g. via variable branching, which induced by ratio of Q/D affected under different light photon flux density, result in structural plasticity. Fig. 7 shows the dynamical growth process of two neighboring trees, using the same parameter file but under anisotropic light condition. Fig. 7(a) - Fig. 7(d) show the 3D visualization of two neighboring trees competing for light at 22 GC, 24 GC, 26 GC, 28 GC, respectively. Fig. 7(e) and Fig. 7(f) show the topology and light intensity at plant age 28 GC respectively.

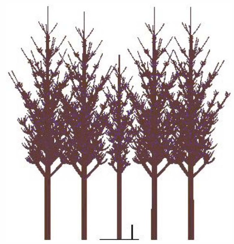

(a) Trees grown with high plant density.

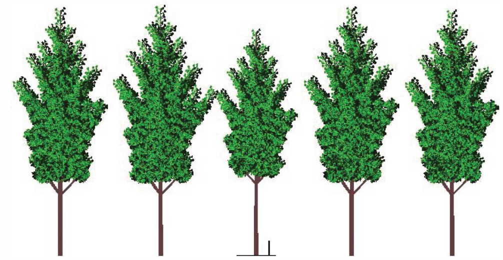

(b) Trees grown with low plant density.

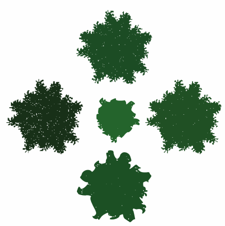

(c)

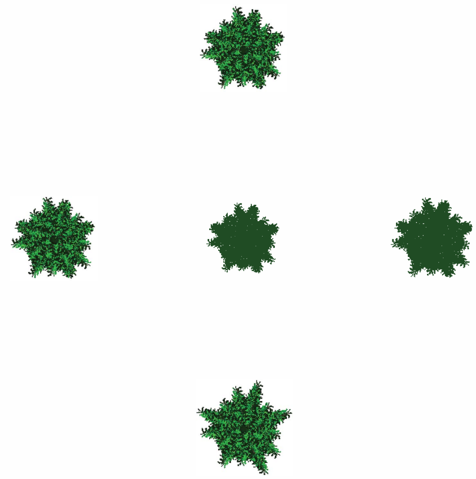

(d)

Figure 6. Trees grown with high plant density (a,c) and low plant density (b,d), under isotropic light source as in Fig. 1

IV. Discussion

Compared with the other light distribution model, Photon Mapping as our technical solution for computing light environment, have some advantages:

1. In trees, source organs, i.e. blades has small size relative to the whole plant. An emitted ray from distance has low probability of striking a small blade, especially at the initial stage of growth. In ray tracing algorithm, it will be necessary to cast huge number of rays into the scene, which costs too much time in collision detection. Photon Mapping algorithm, however, evaluates the light intensity by making use of neighboring photons, which require less ray samples compared to ray tracing algorithm.
2. Photon Mapping algorithm can handle with some physical phenomena, such as caustics, which also happen on translucent blades. In future work, this method is to be used not only in computing biomass production but also in visualization of plants.

This method can simulate the light interception and reflect the coadjustment between plant morphology and local environment. It is helpful for both the graphics applications and tree growth modeling.

In this work, leaves are regarded as round disc in computing light interception, without consideration of leaf geometrical shape. In case that the number of leaves is enormous and leaf size is relatively small compared to full plant structure, this simplification is acceptable. However, when it is applied to crops with big leaves, the collision detection process will be more costly. When light intensity is evaluated by the photons on the leaves instead of photons around the leaves, this method is close the classical ray tracing method.

V. Conclusion

In this paper, we integrated light interception and photosynthesis model into GreenLab model. The result shows that plant plasticity can be simulated under different light environment, through a source-sink approach. Illumination environment could be mimicked by photon mapping method.

Future work includes accurate estimation of light interception for sophisticated geometric structure. This method provide an alternative way of computing biomass production aside Beer-Law approach, which is useful when the aim is to simulate the effect of geometrical structure on light interception and plant growth, or to produce unsymmetrical tree crown for landscape design.

(a) 3D visualization at plant age 22 GC.

(b) 3D visualization at plant age 24 GC.

(c) 3D visualization at plant age 26 GC.

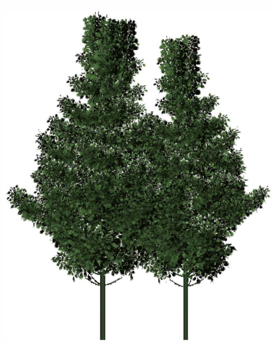

(d) 3D visualization at plant age 28 GC.

(e) Topology at plant age 28 GC.

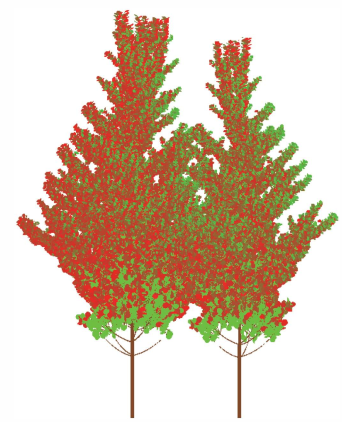

(f) Light intensity at plant age 28 GC.

Figure 7. Two neighboring trees competing for light.

REFERENCES

[1] E. Heuvelink, "Dry matter production in a tomato crop: measurements and simulation," *Annals of Botany*, vol. 75, no. 4, pp. 369–379, 1995.

[2] C. Soler, F. Sillion, F. Blaise, and P. de reffye, "An efficient instantiation algorithm for simulating radiant energy transfer in plant models," *ACM Transactions on Graphics (TOG)*, vol. 22, no. 2, pp. 204–233, 2003.

[3] J. Vos, J. Evers, G. Buck-Sorlin, B. Andrieu, M. Chelle, and P. De Visser, "Functional–structural plant modelling: a new versatile tool in crop science," *Journal of Experimental Botany*, vol. 61, no. 8, pp. 2101–2115, 2010.

[4] J. Dauzat, P. Clouvel, D. Luquet, and P. Martin, "Using virtual plants to analyse the light-foraging efficiency of a low-density cotton crop," *Annals of botany*, vol. 101, no. 8, pp. 1153–1166, 2008.

[5] B. Zheng, L. Shi, Y. Ma, Q. Deng, B. Li, and Y. Guo, "Comparison of architecture among different cultivars of hybrid rice using a spatial light model based on 3-D digitising," *Functional Plant Biology*, vol. 35, no. 10, pp. 900–910, 2008.

[6] X. Wang, Y. Guo, B. Li, X. Wang, and Y. Ma, "Evaluating a three dimensional model of diffuse photosynthetically active radiation in maize canopies," *International Journal of Biometeorology*, vol. 50, no. 6, pp. 349–357, 2006.

[7] B. Zheng, Y. Ma, B. Li, Y. Guo, and Q. Deng, "Assessment of the influence of global dimming on the photosynthetic production of rice based on three-dimensional modeling," *Science China Earth Sciences*, vol. 54, no. 2, pp. 290–297, 2011.

[8] K. Chenu, H. Rey, J. Dauzat, G. Lydie, and J. Lecœur, "Estimation of light interception in research environments: a joint approach using directional light sensors and 3D virtual plants applied to sunflower (helianthus annuus) and arabidopsis thaliana in natural and artificial conditions," *Functional Plant Biology*, vol. 35, no. 10, pp. 850–866, 2008.

[9] J. Evers, J. Vos, B. Andrieu, and P. Struik, "Cessation of tillering in spring wheat in relation to light interception and red: far-red ratio," *Annals of Botany*, vol. 97, no. 4, pp. 649–658, 2006.

[10] K. Kahlen, D. Wiechers, and H. Stützel, "Modelling leaf phototropism in a cucumber canopy," *Functional Plant Biology*, vol. 35, no. 10, pp. 876–884, 2008.

[11] P. Cournède, A. Mathieu, F. Houllier, D. Barthélémy, and P. de Reffye, "Computing competition for light in the greenlab model of plant growth: a contribution to the study of the effects of density on resource acquisition and architectural development," *Annals of Botany*, vol. 101, no. 8, pp. 1207–1219, 2008.

[12] W. Palubicki, K. Horel, S. Longay, A. Runions, B. Lane, R. Měch, and P. Prusinkiewicz, "Self-organizing tree models for image synthesis," in *ACM Transactions on Graphics (TOG)*, vol. 28, no. 3, 2009, pp. 58–68.

[13] J. Hua and M. Kang, "Functional tree models reacting to the environment," in *ACM SIGGRAPH 2011*. ACM, 2011, p. 60.

[14] H. Jensen, *Realistic image synthesis using photon mapping*. AK Peters, Ltd., 2001.

[15] M. Kang, L. Yang, B. Zhang, and P. de Reffye, "Correlation between dynamic tomato fruit-set and source–sink ratio: a common relationship for different plant densities and seasons?" *Annals of Botany*, vol. 107, no. 5, pp. 805–815, 2011.

[16] V. Letort, P. Cournède, A. Mathieu, P. de Reffye, and T. Constant, "Parametric identification of a functional–structural tree growth model and application to beech trees (fagus sylvatica)," *Functional Plant Biology*, vol. 35, no. 10, pp. 951–963, 2008.

[17] P. Shirley and R. Morley, *Realistic ray tracing*. AK Peters, Ltd., 2003.

[18] D. Falster and M. Westoby, "Leaf size and angle vary widely across species: what consequences for light interception?" *New Phytologist*, vol. 158, no. 3, pp. 509–525, 2003.

[19] Z. Zhu, X. Sun, G. Yu, X. Wen, Y. Zhang, S. Han, J. Yan, and H. Wang, "Radiometers performance attenuation and data correction in long term observation of total radiation and photosynthetically active radiation in typical forest ecosystems in china," *Chinese Journal of Applied Ecology*, vol. 22, no. 11, pp. 2954–2962, 2011.

[20] J. Ehleringer and R. Pearcy, "Variation in quantum yield for CO2 uptake among C3 and C4 plants," *Plant Physiology*, vol. 73, no. 3, pp. 555–559, 1983.

[21] T. Givnish, "Adaptation to sun and shade: a whole-plant perspective," *Functional Plant Biology*, vol. 15, no. 2, pp. 63–92, 1988.

[22] A. Gaweda, A. Jacobs, M. Brier, and J. Zurada, "Pharmacodynamic population analysis in chronic renal failure using artificial neural networks–a comparative study," *Neural Networks*, vol. 16, no. 5-6, pp. 841–845, 2003.